# Photoresponse of the AlN-based SAW device on polymeric and silicon substrates.

Leonardo Lamanna\*,1,2,3, Francesco Rizzi<sup>1</sup>, Marco Bianco<sup>1,2</sup>, Matteo Agostini<sup>4</sup>, Marco Cecchini<sup>4</sup>, Massimo De Vittorio<sup>1,2,a</sup>, Venkat R. Bhethanabotla<sup>3, a</sup>.

<sup>1</sup> Center for Biomolecular Nanotechnologies, Istituto Italiano di Tecnologia, Via Barsanti snc, Arnesano, Italy
<sup>2</sup> University of Salento, Department of Innovation Engineering, Campus Ecotekne, Via Monteroni, Lecce, Italy
<sup>3</sup> Department of Chemical & Biomedical Engineering University of South Florida Tampa, USA
<sup>4</sup>NEST, IstitutoNanoscienze-CNR and Scuola Normale Superiore, Piazza San Silvestro 12, Pisa, Italy
<sup>a</sup> These authors jointly supervised this work
\*leonardo.lamanna@iit.it;

Abstract— This paper shows the optical photoresponse in the IR-Vis-UV range of a AlN-based piezoelectric surface acoustic wave (SAW) delay-line device. The piezoelectric aluminum nitride (AlN) thin film has been sputtered on both silicon rigid substrate and flexible polyethylene naphthalate (PEN) substrate. Both devices have been investigated in their electroacoustic response, by measuring the transfer function S21 and by laser Doppler vibrometer characterization. The silicon based SAW devices, stimulated by the IR-Vis-UV light, are strongly affected in the out-of-band insertion loss due to the photovoltaic effect. A mathematical model has been implemented to correlate the out-of-band loss with the material's electrical admittance change. In contrast PEN based SAW devices, due to the polymeric nature of the substrate, did not show any variation in the out-of-band loss.

Moreover, when exposed to UV light, a frequency downshift of the Rayleigh and Lamb resonances modes have been observed in all the devices, due screening of the photoinduced electrons in the AlN piezoelectric layer which induces an acoustic wave velocity reduction. To the best of our knowledge, this is the first photoresponse study exploiting SAW in the range IR-Vis-UV, suggesting a new detection mode of UV light by a flexible AlN based SAW device. Further development of these devices can lead to a new class of light sensors from UV to IR, based on remote SAW devices.

Keywords— AlN thin film, UV-vis-IR sensing, flexible SAW devices.

## I. INTRODUCTION

Surface acoustic wave (SAW) devices represent one of the most widely used micro electro mechanical systems (MEMS). The versatility of application of a SAW device is based on features such as low cost, small size, high reliability, good reproducibility and their wireless control capability[1-3]. SAW devices fabricated on piezoelectric thin films represent the most promising technology easily integrable in sensors, transducers, and lab on chip systems [4]. The main materials involved in this class of devices are zinc oxide (ZnO) and aluminum nitride (AlN). In particular, AlN represents an excellent substrate for the SAW device microfabrication thanks to good piezoelectric and dielectric properties, complementary-metal-oxide-semiconductor (CMOS) processing compatibility and biocompatibility [4, 5]. Moreover, the high SAW propagation velocity and high breakdown voltage allow the fabrication of devices working with high power and in the GHz range [4, 6]. Recently, improvement in the sputtering technique allowed deposition of c-axis orientated AlN films at low temperature on different substrates such as sapphire [7], LiNbO<sub>3</sub> [8, 9], silicon [10] and polymers[6, 11-13].

The modes and amplitude of the waves propagation in the AlN-based SAW device, are strictly related to the electrical and mechanical properties of the substrate[4, 6, 11]. In particular, c-axis (0002) orientated Aluminum Nitride allows two principal wave propagation modes in SAW devices: Rayleigh waves (R-SAWs) and Lamb waves (L-SAWs). The R-SAWs are favored in the AlN grown on rigid substrates (usually silicon) with a phase velocity of about 5000 m/s; instead, the L-SAWs, traveling at a phase velocity of about 10000 m/s, are favored in AlN membranes and in AlN thin films grown on polymeric soft substrates [4, 6, 11].

In this work, the interaction of light radiation with the SAW passive substrate and with the piezoelectric AlN active layer has been investigated by exploiting silicon and polymeric polyethylene naphthalate (PEN) substrates. Silicon is the most common substrate used in integrated electronics; it is a semiconductor with indirect bandgap energy around 1.14 eV at room temperature, and when photon-stimulated above, it shows a photovoltaic effect with a consequent resistivity change[14-16]. The resistivity change of the substrate influences the SAW device performance, mostly due to the electrical feedthrough between the interdigital transducers (IDTs), which considerably change the out-of-band signal [10]. In a sinusoidal voltage regime (AC circuits), the SAW resistance is described as a complex impedance or admittance [17]. In this study, the change of the admittance has been reported as a function of the different wavelength stimulus. Since the transmission signal S<sub>21</sub> is influenced by feedthrough in the silicon substrate, a theoretical model has been developed to parameterize the out-of-band insertion loss with the characteristic material admittance. This behavior has been compared with SAW devices fabricated on polymeric PEN substrate, whose electrical properties are not affected by light stimulation. Finally, AlN light sensitivity of the SAW resonances have been investigated. Devices stimulated by UV light have shown a change in the resonance frequency due to the screening of the piezoelectric fields with a consequent reduction of the acoustic wave velocity [18]. The SAW device response to different radiation wavelengths, shows a very good agreement with the theoretical model. The knowledge of SAWs modes propagation and the development of theoretical models describing the influence of external physical parameters on their propagation is an important step for designing a SAW-based sensor. This study allows to envision a new class of SAW -based light sensing devices that will find application in different fields such as flame monitors, sunlight meters, photochemical phenomena detectors, etc.

An earlier version of this paper was presented at the IEEE sensors 2019 in Montreal, Canada and was published in its Proceedings. DOI: 10.1109/SENSORS43011.2019.8956526

## II. MATERIALS, DEPOSITION AND FABRICATION

Silicon (1000  $\Omega$ /cm) with a top layer of SiN (10000  $\Omega$ /cm) substrate was purchased from Si-Mat; Polyethylene Naphthalate (PEN) film of 125 µm thickness was purchased from Teonex.

The AlN deposition was carried out according to Lamanna et al. [6] on silicon and PEN; it will be briefly outlined here. Multistep AlN sputtering growth has been carried out in order to deposit 4.5 µm of piezoelectric AlN. The growth shows high c-axis crystal orientation with an average grain size of 50 nm, surface roughness of approximately 7.5 nm and effective piezoelectric coefficient of 3.3 pm/V [6]. The devices used in the present study are delay lines constituted by two identical metal interdigital transducers (IDT) whose purpose is the generation of the SAWs[4, 6]. Each delay line is designed with 40 pairs of fingers,  $\lambda$ =20 $\mu$ m with a metallization ratio of 0.5, an acoustic aperture of 400  $\mu m$  and a delay line of 20  $\lambda$ . Fig.1a shows the unit-cell diagram of the SAW device. The microfabrication of the IDTs pattern is improved with respect to the previous work, exploiting a lift-off photolithography process using AZ 5214 E Image Reversal Photoresist. The metallization was carried out with a thermal evaporator using aluminum pellets (99.95% pure) with a final thickness of around 1000 Angstroms. In fact, the lift-off process preserves a low surface roughness of the sputtered AlN [12], irreparably damaged with dry or wet etching processing. Moreover, the use of aluminum as IDTs metal has the advantage of a surface acoustic energy confinement [4].

## III. EXPERIMENTAL

The transfer function S21 has been obtained at room temperature with a vector network analyzer (Agilent 8753ES) using |Z|Probe with 150 µm pitch. The experimental set up, used to study the electroacoustic photoresponse of the SAW devices, is shown in Fig.1b. For the sensing tests, the light source was fixed at 3 cm from the delay line. The light sources used in the work are LEDs of wavelengths: 365nm (code M365LP1), 530nm (code M530L4), 660nm (code M660L4) and 940 nm (code M940L3) all purchased from Thorlabs. The LEDs were controlled by a T-Cube<sup>TM</sup> LED Driver purchased from Thorlabs. The power of the light source for the different wavelength is reported according to Thorlabs datasheet in Table 1.

LEDS WAVELENGTHS, EQUIVALENT EV ENERGY AND TABLE I. LEDS OUTPUT POWER IN ACCORDING TO THORLABS DATASHEETS.

nm	eV	mW
365	3.5	1150
530	2.4	350
660	1.9	940
940	1.3	800

Moreover, in the NIR spectral region the sample has been irradiated laser fs-pulses with wavelengths in a range of 900-1225 nm (scanning steps of 25 nm), with the laser power kept constant at 600 mW.

The laser Doppler measurements were performed by using a vibrometer UHF-120 Ultra High Frequency Vibrometer (Polytec, Germany). The employed scanning (laser Doppler vibrometer) LDV system enables non-contact measurements in real time for the characterization of out-of-plane SAW

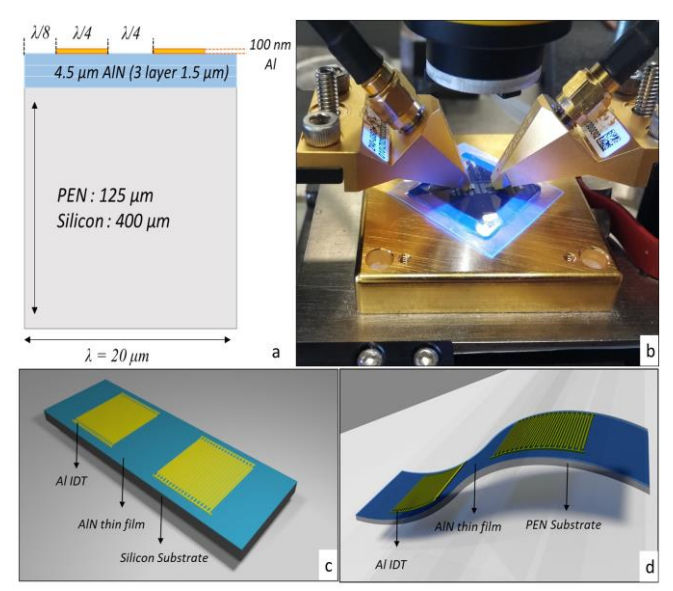


Fig. 1: a) Unit cell diagram of the SAW device; b) Experimental set up for electroacoustic photoresponse test; c,d) 3D schematic of the developed AlNbased SAW device on Silicon and flexible Polyethylene Naphthalate substrate, respectively.

amplitude of displacement at any sample point (vertical resolution of a few tens of picometers) [19]. Single frequency scan spectra have been collected averaging 5 spectra at the resonance frequency, by appling 5V AC signal, at the Rayleigh and Lamb resonance frequency on both the substrates. The detection array has been built with a point density of  $\approx$  1.6 µm along the perpendicular direction, and  $\approx$ 5 µm along the parallel direction to the wavefront.

# IV. MODELING

To characterize the out-of-band signal as a function of the incident light and therefore exploiting the electrical admittance, the two port reciprocal network model proposed by Clement et al. [10, 20] was implemented (Fig.2).

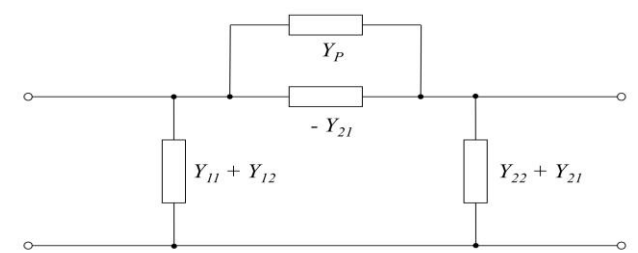


Fig. 2: Equivalent circuits for a reciprocal two-port network, with the implementation of the feedthrough effect Y<sub>P</sub>.

The admittance coefficient for a delay line spaced by  $n\lambda$  is given by:

$$Y_{11} = Y_{22} = G + j(B + \omega_0 C_{tot}) \tag{1}$$

$$Y_{21} = Y_{12} = G + exp(-j\omega_0 \frac{n\lambda}{f_0})$$
 (2)

$$G = \frac{4}{\pi} k^2 \omega_0 C_{tot} N \left(\frac{\sin(x)}{x}\right)^2$$
 (3)

$$Y_{11=}Y_{22} = G + j(B + \omega_0 C_{tot})$$
(1)  

$$Y_{21=}Y_{12} = G + exp(-j\omega_0 \frac{n\lambda}{f_0})$$
(2)  

$$G = \frac{4}{\pi}k^2 \omega_0 C_{tot} N(\frac{\sin(x)}{x})^2$$
(3)  

$$B = \frac{4}{\pi}k^2 \omega_0 C_{tot} N(\frac{\sin(2x) - 2x}{2x^2})$$
(4)

where B is the conductance, G is susceptance,  $C_{tot}$  is the IDT capacitance empirically fitted,  $\omega$  the angular frequency,  $\omega_0$  angular resonance frequency, N pair of finger,  $K^2$  is the

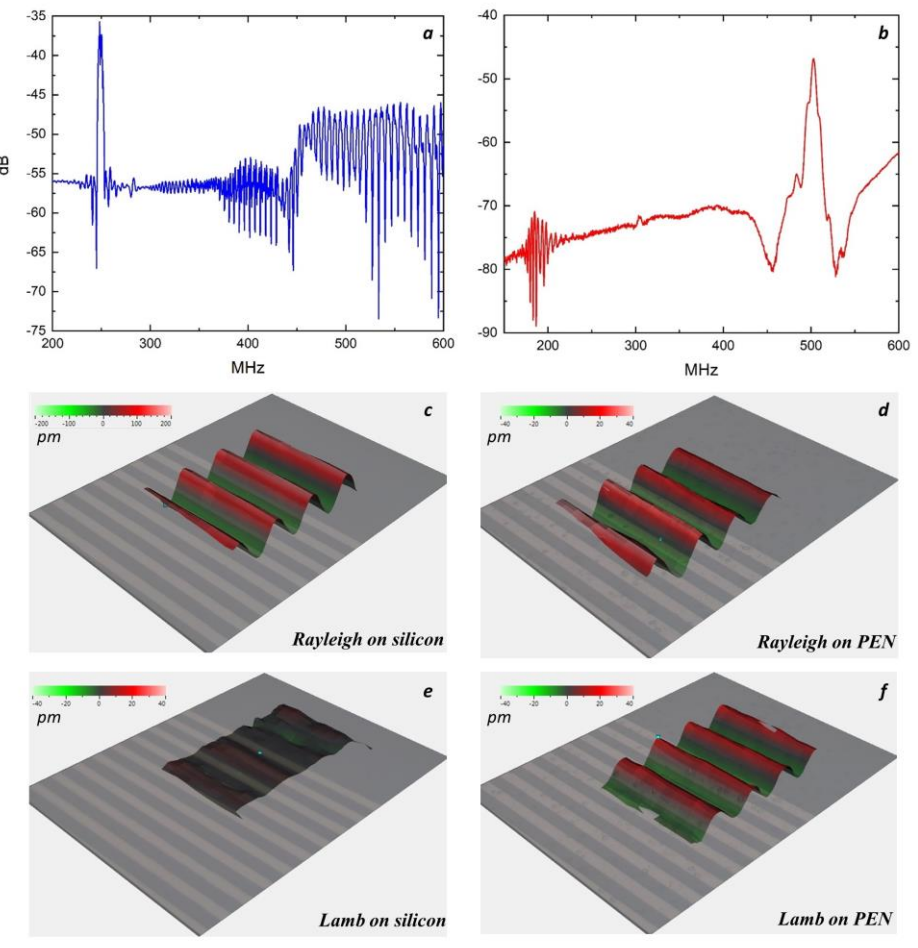


Fig. 3:a,b) Transfer function amplitude S<sub>21</sub> of devices fabricated on silicon and PEN substrate, respectively; c,d)Representative LDV 2D frames of the Rayleigh traveling waves on silicon and PEN, respectively; e,f) Representative LDV 2D frames of the Lamb traveling waves on silicon and PEN, respectively.

electromechanical coupling equal to 0.85 as calculated in the previous work [6] and x is calculated as  $[N\pi ((\omega-\omega_0)/\omega_0)]$ .

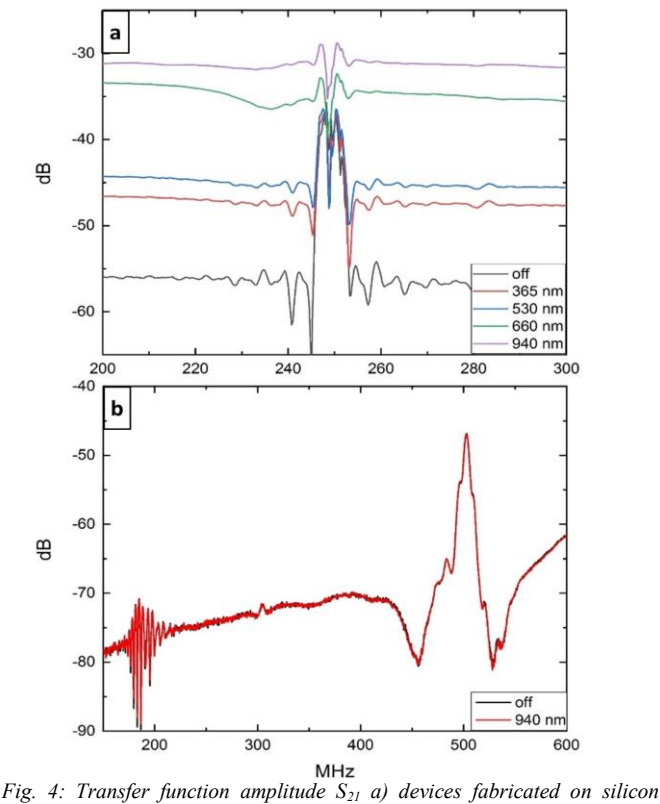
The transfer function  $S_{21}$  is given by:

$$S_{21} = \frac{-2 Y_{21} Y_0}{(Y_0 + Y_{11})^2 - Y_{21}^2} \tag{5}$$

where  $Y_0$  represents the admittance in agreement with the experimental setup. To fit the experimental data with the mathematical model, the feedthrough has to be calculated. According to [10] these effects can be approximated by adding a real term  $Y_P$  to  $Y_{21}$  parameter, which is equivalent to a purely resistive admittance in parallel. In an ideal case with a zero resistive admittance of the material, the response is a perfect *sinc* function signal (Fig.6a).

## V. DISCUSSION

Preliminarily, the devices were tested by measuring the transmission amplitude signal  $S_{21}$  (Fig. 3 a,b), identifying the Rayleigh and Lamb resonance modes. The SAW devices fabricated on silicon substrate show a Rayleigh mode propagation (Fig. 3a) with a resonant frequency at 252 MHz and a spurious signal band at higher frequencies (centered at 540 MHz) corresponding to a Lamb wave propagation [6]. Instead, the SAW devices fabricated on PEN (Fig. 3b) exhibit two clear resonance modes: Rayleigh at a lower frequency (185 MHz) and symmetric Lamb  $S_0$  at a higher frequency (502



substrate stimulated by different wavelengths light; b) devices fabricated on PEN substrate without light exposure and stimulated by IR light.

MHz), in accordance with the previous work and the theoretical wave velocity [6]. To inspect the transversal component at different SAW deformation modes, laser Doppler vibrometry (LDV) has been exploited. With the aim of observing the surface acoustic wave propagation, a frames of the oscillating surface are reported in fig 3. c-f (and the videos are in the supplementary section). Such modes are close to the FEM based simulation reported in our previous works [6, 11]. Rayleigh wave propagation show a higher transversal displacement and lower damping on silicon (fig. 3c) with respect to PEN substrate (fig. 3d). In contrast, the Lamb waves present higher displacement on PEN with respect silicon and lower damping, confirming the electroacoustic measurements (fig. 3 a,b) and SAW propagation theory [3,5]. Noteworthy, the measured displacement for the Lamb wave should be considered half of the whole deformation since the S<sub>0</sub> Lamb waves own a symmetrical deformation in the lower interface [4, 21].

The characterization of the transfer functions S<sub>21</sub>, after UV-Vis-IR excitation, is reported in Fig. 4. Fig. 4a shows how the exposure of the silicon-SAW devices at different wavelengths changes the out-of-band insertion loss. As observed with the LED excitation, the wavelength increase corresponds to an increase of the out-of-band losses with a maximum at 940 nm, close to silicon band indirect gap. This is strictly linked to the different amount of charge generation at different wavelengths [22, 23]. This charge is capacitively induced at the interface with the piezoelectric AlN, producing a consequent increasing of the electrical feedthrough between the IDTs.

To investigate the maximum in the out of band loss close to the silicon indirect energy gap around 1.14eV (1080 nm), the device has been excited by tunable laser in the NIR region (900-1225 nm). In fig. 5 the out-of-band magnitude as a function to the laser incident wavelengths is reported. It is

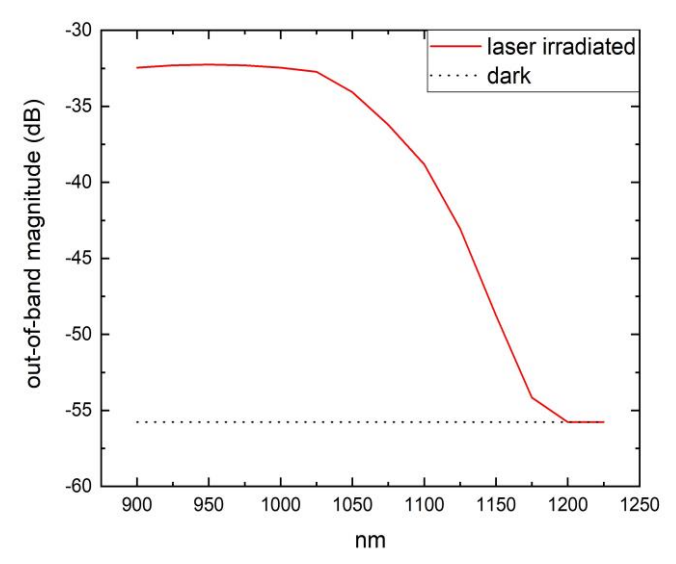


Fig. 5: Out-of-band magnitude measurements in silicon-based SAW devices irradiated by NIR laser

shown a decrease of the out-of-band magnitude at wavelengths higher than 1050nm, recovering the out-of-band dark condition at wavelength higher than 1200 nm. Therefore, at room temperature, the electrons promotion in the conduction band is favored when the incident radiation energy increases towards the indirect bandgap energy value with a consequent silicon resistivity change[23-25]. In silicon, the indirect energy bandgap semiconductors such as silicon, in the NIR, optical transitions of electrons to conduction band require a change in both energy and momentum mediated by interactions with phonons which are abundant at room temperature, generating the feed-through between IDTs [24].

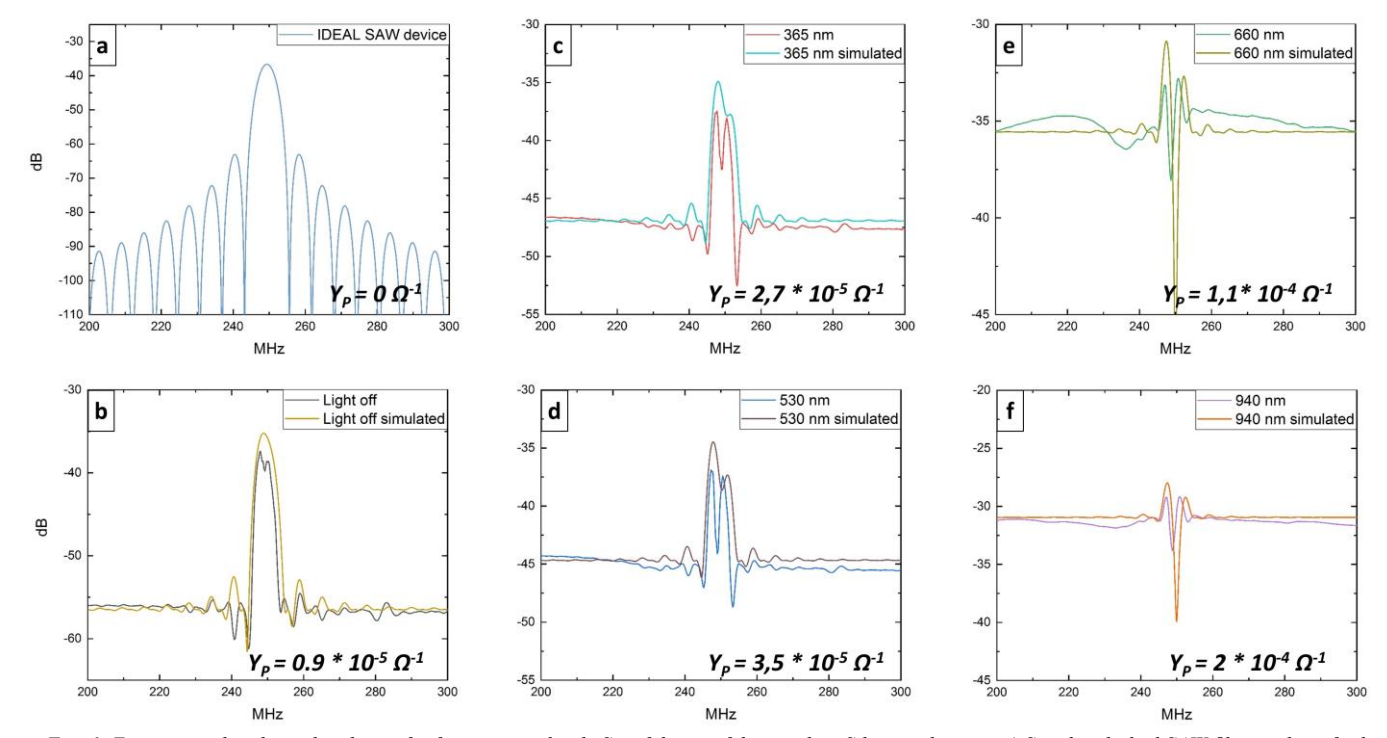


Fig. 6: Experimental and simulated transfer function amplitude  $S_{21}$  of devices fabricated on Silicon substrate: a) Simulated ideal SAW filter without feed-through; b) comparison of experimental and simulated data of device without light stimulus; c,d,e,f) comparison of experimental and simulated data of devices stimulated by 365nm, 530nm, 660nm, 940nm LEDs, respectively.

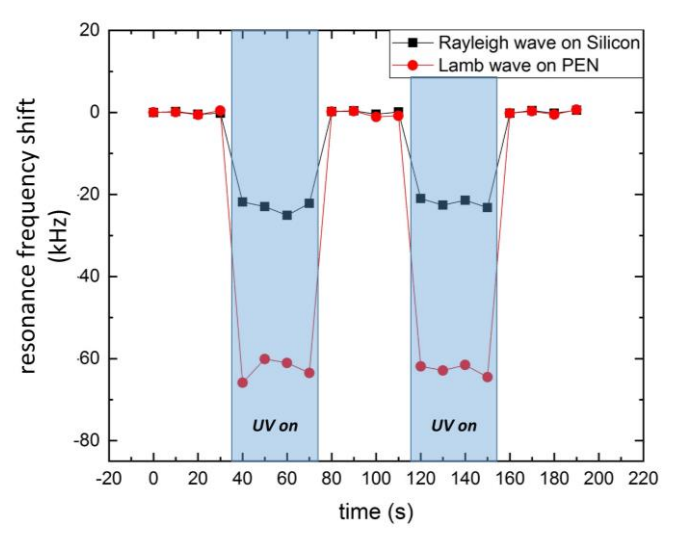


Fig. 7: Real-time resonance shift of Lamb and Rayleigh modes in AlN-based SAW devices exploited as UV detector under 365nm LED source.

This effect is not present in the devices fabricated on PEN polymeric substrate, transparent to these radiation wavelengths range and therefore not showing out-of-band insertion loss changes; the two curves are overlapped (Fig. 4b). Fig.6 shows the  $S_{21}$  spectra measured with different incident light stimuli and the relative  $S_{21}$  simulated spectra with different resistive admittance added to an ideal AlN-based SAW filter on silicon ( $Y_P$ ). The theoretical model perfectly fits the experimental data. This simple model provides valuable information about the change of electrical property of the substrate. In fact, it shows how the substrate admittance changes in a range between 0.8  $10^{-5} \Omega^{-1}$  to 2  $10^{-4} \Omega^{-1}$ , as it happens when it is stimulated by different wavelengths LED sources. This variation is in good agreement with the literature [26, 27].

The resonance frequency has been characterized for all the devices stimulated by different wavelengths. A shift is observed only when the devices have been stimulated by a 365nm light source (Fig. 7) while no resonance shift is observed with the other wavelengths. This behavior is due to the large direct bandgap of AlN which makes it sensitive only in the UV light range [28]. In fact, the photoinduced electrons in the AlN screen the piezoelectric field and reduce the acoustic velocity [18]. The change of the SAW velocity can be expressed as:

$$\frac{\Delta v}{v_0} = \frac{K^2}{2\left(1 + \left(\frac{\sigma}{\sigma_m}\right)^2\right)} \tag{6}$$

where  $v_{\theta}$  is the SAW velocity on a free surface,  $K^2$  is the electro-mechanical coupling coefficient,  $\sigma$  is the sheet conductivity, and  $\sigma_m$  is a material constant. Therefore, the resonance frequency shift is due to the reduction of the acoustic wave velocity by the increase of photo-induced conductivity of AlN film[18, 28, 29]. Such resonance shift is not observed at higher wavelengths (IR-vis), due to the low energy of the electromagnetic radiation in that spectral range, which does not allow the electron promotion in the AlN. In contrast, IR-vis wavelengths affect just the silicon substrate as shown in fig.4, and do not influence the electromechanical properties of the AlN.

A larger shift is reported for the Lamb wave on PEN substrate (~60 kHz) compared to the silicon substrate (~20

kHz). Noteworthy, the resonance frequency goes back to the initial value after the UV source has been turned off for both resonances. To the best of our knowledge, this is the first detection of UV light with a flexible AlN based SAW device.

## VI. CONCLUSIONS

In this work non-contact optical measurements, by a laser Doppler vibrometer, have been exploited to measure the transversal displacement in the Rayleigh and Lamb wave propagation on AlN-based SAW delay line fabricated on silicon and polyethylene naphthalate. The results have confirmed the electroacoustic measurements and SAW propagation theory in both.

The photoresponse, of these SAW delay line, has been investigated in the UV-vis-IR range. The transfer functions S<sub>21</sub> are affected significantly when the devices are stimulated by the light. In fact, the devices fabricated on silicon, stimulated by light, showed an enhanced change in the out-of-band signal at near IR while the device fabricated on the PEN flexible substrate does not undergo any variation, envisioning silicon based SAW as an IR sensor. A mathematical model has been implemented to calculate the admittance change as a function of the wavelength light stimulus, achieving an optimal fit for all experimental data. This model, exploited for silicon, could be used for a wide range of semiconductor based SAW devices using different energy bandgap to implement sensitivity for different wavelength. Finally, the Rayleigh and Lamb resonance frequency down-shift has been observed in the UV range, due to the screening of the AlN piezoelectric fields with a consequent reduction of the acoustic wave velocity. In particular, the exploitation of PEN based SAW devices enhances the resonance shift improving the responsivity to the UV light.

The development of theoretical models and SAW devices sensitive to different power and wavelength light paves the way for a new class of remote device, which could find applications in different fields such as flame monitors, sunlight exposure meters, photochemical phenomena detectors, etc.

## **ACKNOWLEDGMENTS**

This work was partially funded by the National Science Foundation (Grant No. IIP-1640668), which is gratefully acknowledged.

## REFERENCES

- [1] V. P. Plessky and L. M. Reindl, "Review on SAW RFID tags," *IEEE transactions on ultrasonics, ferroelectrics, and frequency control,* vol. 57, no. 3, pp. 654-668, 2010.
- [2] A. Pohl, "A review of wireless SAW sensors," *IEEE transactions on ultrasonics, ferroelectrics, and frequency control*, vol. 47, no. 2, pp. 317-332, 2000.
- [3] I. Marasco *et al.*, "Compact and flexible meander antenna for Surface Acoustic Wave sensors," *Microelectronic Engineering*, p. 111322, 2020.
- [4] Y. Q. Fu *et al.*, "Advances in piezoelectric thin films for acoustic biosensors, acoustofluidics and lab-on-chip applications," *Progress in Materials Science*, vol. 89, pp. 31-91, 2017.

- [5] G. Iriarte, J. Rodríguez, and F. Calle, "Synthesis of c-axis oriented AlN thin films on different substrates: A review," *Materials Research Bulletin*, vol. 45, no. 9, pp. 1039-1045, 2010.
- [6] L. Lamanna et al., "Flexible and Transparent Aluminum Nitride Based Surface Acoustic Wave Device on Polymeric Polyethylene Naphthalate," Advanced Electronic Materials, p. 1900095, 2019.
- [7] Y. Ohba and A. Hatano, "Growth of high-quality AlN and AlN/GaN/AlN heterostructure on sapphire substrate," *Japanese journal of applied physics*, vol. 35, no. 8B, p. L1013, 1996.
- [8] G. T. Hwang, M. Byun, C. K. Jeong, and K. J. Lee, "Flexible Piezoelectric Thin - Film Energy Harvesters and Nanosensors for Biomedical Applications," *Advanced healthcare materials*, vol. 4, no. 5, pp. 646-658, 2015.
- [9] P. K. Das, A. D. Snider, and V. R. Bhethanabotla, "Acoustothermal heating in surface acoustic wave driven microchannel flow," *Physics of Fluids*, vol. 31, no. 10, p. 106106, 2019.
- [10] M. Clement, L. Vergara, J. Sangrador, E. Iborra, and A. Sanz-Hervás, "SAW characteristics of AlN films sputtered on silicon substrates," *Ultrasonics*, vol. 42, no. 1-9, pp. 403-407, 2004.
- [11] L. Lamanna, F. Rizzi, V. R. Bhethanabotla, and M. De Vittorio, "Conformable surface acoustic wave biosensor for E-coli fabricated on PEN plastic film," *Biosensors and Bioelectronics*, p. 112164, 2020.
- [12] L. Lamanna, F. Rizzi, M. De Vittorio, and V. R. Bhethanabotla, "Light interaction with AlN-based SAW device fabricated on flexible and silicon substrate," in 2019 IEEE SENSORS, 2019, pp. 1-4: IEEE
- [13] F. Guido, A. Qualtieri, L. Algieri, E. D. Lemma, M. De Vittorio, and M. T. Todaro, "AlN-based flexible piezoelectric skin for energy harvesting from human motion," *Microelectronic Engineering*, vol. 159, pp. 174-178, 2016.
- [14] Y. A. Vlasov, X.-Z. Bo, J. C. Sturm, and D. J. Norris, "On-chip natural assembly of silicon photonic bandgap crystals," *Nature*, vol. 414, no. 6861, p. 289, 2001.
- [15] P. A. Schultz, "Theory of defect levels and the "band gap problem" in silicon," *Physical review letters*, vol. 96, no. 24, p. 246401, 2006.
- [16] J. J. Loferski, "Theoretical considerations governing the choice of the optimum semiconductor for photovoltaic solar energy conversion," *Journal of Applied Physics*, vol. 27, no. 7, pp. 777-784, 1956.

- [17] L. Callegaro, *Electrical impedance: principles, measurement, and applications.* CRC Press, 2012.
- [18] M. R. Chen, S. Chang, T. C. Chen, C. H. Hsu, H. Kao, and J. I. Chyi, "Fabrication study of AlN solar blind (< 280 nm) MSM photodetectors grown by low temperature deposition," *physica status solidi (a)*, vol. 207, no. 1, pp. 224-228, 2010.
- [19] C. Accoto *et al.*, "Two-photon polymerization lithography and laser doppler vibrometry of a SU-8-based suspended microchannel resonator," *Journal of Microelectromechanical Systems*, vol. 24, no. 4, pp. 1038-1042, 2014.
- [20] D. M. Pozar, *Microwave engineering*. John Wiley & Sons, 2009.
- [21] H. Lamb, "On waves in an elastic plate," *Proc. R. Soc. Lond. A*, vol. 93, no. 648, pp. 114-128, 1917.
- [22] K. Rajkanan, R. Singh, and J. Shewchun, "Absorption coefficient of silicon for solar cell calculations," *Solid-State Electronics*, vol. 22, no. 9, pp. 793-795, 1979.
- [23] S. M. Sze, Semiconductor devices: physics and technology. John wiley & sons, 2008.
- [24] J. Pankove, "Optical processes on semiconductors Dover publication," *Inc. New york*, 1971.
- [25] W. S. Yoo, K. Kang, G. Murai, and M. Yoshimoto, "Temperature dependence of photoluminescence spectra from crystalline silicon," *ECS Journal of Solid State Science and Technology*, vol. 4, no. 12, pp. P456-P461, 2015.
- [26] S. Kumar, P. Singh, and G. Chilana, "Study of silicon solar cell at different intensities of illumination and wavelengths using impedance spectroscopy," *Solar Energy Materials and Solar Cells*, vol. 93, no. 10, pp. 1881-1884, 2009.
- [27] L. Raniero, E. Fortunato, I. Ferreira, and R. Martins, "Study of nanostructured/amorphous silicon solar cell by impedance spectroscopy technique," *Journal of non-crystalline solids*, vol. 352, no. 9-20, pp. 1880-1883, 2006.
- [28] C. P. Laksana *et al.*, "Deep-UVsensors based on SAW oscillators using low-temperature-grown AlN films on sapphires," *IEEE transactions on ultrasonics, ferroelectrics, and frequency control*, vol. 58, no. 8, pp. 1688-1693, 2011.
- [29] D. Ballantine Jr et al., Acoustic wave sensors: theory, design and physico-chemical applications. Elsevier, 1996.